PERFORMANCE OF A CLOSED CYCLE POWER TAKE OFF FOR MUTRIKU BREAKWATER

Morgane Bellec, Ciara Gurhy, Lee Gibson & Craig Meskell
School of Engineering, Trinity College Dublin, Ireland

ABSTRACT

An oscillating water column (OWC) type wave energy converter was installed in Mutriku breakwater (Basque Country, Spain). The wave power is transferred to an air flow that turns a turbine. The facility currently uses self-rectifying turbines. A closed cycle power take off (CCPTO) arrangement, by forcing the flow to be unidirectional, would allow the use of more efficient turbines than currently employed. In this paper, a reduced order model for such a system is introduced. Using Mutriku breakwater dimensions the expected power performance is assessed. The sensitivity of the system to basic geometric features such as turbine and valves sizes is explored using monochromatic ideal wave. It is found that while there is an opimal size turbine, there is no benefit to increasing the valve size beyond a certain area. More realistic sea states representative of Mutriku are investigated using polychromatic waves as an input. The effect of tide is also considered by comparing extreme high and low tide conditions with the mean tide. It is found that tide height has a significant impact on the power production capacity. The trends uncovered by this work will form a useful basis for the design of the actual power take off including the unidirectional turbine.

1. INTRODUCTION

Wave power has long been an attractive potential source of renewable energy due to its high density and availability around the world. Moreover, the resource has good predictability and is decorrelated with wind and solar power, as shown by Fusco et al. (2010). In spite of all those advantages, wave energy is still in infancy, with a large number of concepts at various stages of development. A promising class of device is called the oscillating water column (OWC) in which the wave power is transferred to air flow. Wave energy conversion based on OWC devices whether floating or fixed offers several advantages: the mechanism is not submerged; the sea chamber can provide an effective gearing of the flow; and perhaps the most useful is that the energy presented to the turbine (i.e. in the air) can be dramatically reduced by venting in highly energetic sea states as highlighted by Henriques et al. (2016). However, the main disadvantage is that the flow of air across the turbine is bidirectional i.e. the air flow reverses twice per wave cycle. This has been overcome to some extent with self-rectifying turbines (e.g. Wells, axial impulse or biradial turbines), but these can have poor performance as the rotational speed of the turbine is nearly always mismatched to the instantaneous airflow velocity. A closed cycle power take off (CCPTO) system consisting of two large air reservoirs connected by a unidirectional turbine has been proposed by Vicente et al. (2017). This arrangement was examined for a floating installation in Benreguig et al. (2019).

In the CCPTO arrangement, shown conceptually in Fig. 1, the power take off consists of three air chambers: the sea chamber which is exposed to the OWC, the high pressure (HP) reservoir and the low pressure (LP) reservoir. The sea chamber is connected to the HP and LP reservoirs by non-return valves (designated HP and LP valves respectively), while the HP and LP reservoirs are connected by the air turbine. Whether the sea level in the sea chamber of the OWC is rising or falling, the pressure in the HP reservoir is always above that in the LP reservoir, and so the flow across the turbine is unidirectional. This is the principle benefit of this arrangement.

In order to understand the operation of the Closed Cycle PTO consider the wave cycle as two half-cycles: a compression process and an expansion process. During the compression process, the rising water surface in the sea chamber compresses air raising the pressure, P_1, in this chamber. For a short time both valves are closed. This is not achieved by active control of the valves, but by the temporal variation of the pressure in the three chambers. When the sea chamber pressure rises above the pressure in the HP reservoir, P_2, the HP valve opens while the LP valve remains closed. For the remainder of the compression process the OWC is compressing all of the air in the system through the HP reservoir, turbine and LP reservoir. Due to the pressure drop across the valves and turbine, the LP pressure, P_3 is always lower the the HP pressure, P_2. Hence, the LP valve remains

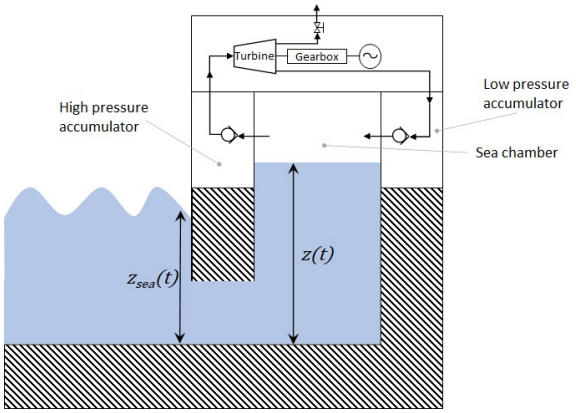

Figure 1. Closed Cycle Power Take Off (CCPTO) for a shore-based installation. Pneumatic path including non-return valves and turbine through the sea, high pressure and low pressure chambers indicated.

closed during the OWC compression process. During expansion, the opposite happens. The sea level drops in the sea chamber, reducing the pressure, until P_1 is below the HP pressure, P_2 which causes the HP valve to shut off. As the pressure P_1 continues to drop, it will fall below the LP pressure, P_3 causing the LP valve to open. From this point on, the expansion process is expanding the air in the HP and LP reservoirs into the sea chamber. The system is nonlinear for two reasons: the compressibility of the air means that the pneumatic spring effect is asymmetric around the equilibrium, with the compression cycle experiencing a harder spring than the expansion; in addition, the opening of the valves represents a softening spring effect. Furthermore, the triggering of the valve opening depends not just on the instantaneous pressure within the sea chamber, but also the time history of the discharge from the high pressure chamber, introducing a memory effect. Indeed the pressure difference needed to trigger the valve is actually bigger than the one needed to keep it open, so the valve position (open or close) at each time also depends on its past positions. Thus, it is necessary to model the CCPTO in the time domain, although this latter memory effect is not yet considered in the present study. In this paper, a reduced order model for a CCPTO is introduced and applied to a notional shore based installation which would be compatible with Mutriku breakwater. The objective is to assess the sensitivity of the power available in a CCPTO to the size of valves and turbine for a range of sea states and tide heights. The term size is here understood as a global metric that serves as a proxy for the power production capacity; in effect it includes the physical sizes, the rotational speed and the operating conditions of the turbine and valves. Mutriku is a fixed

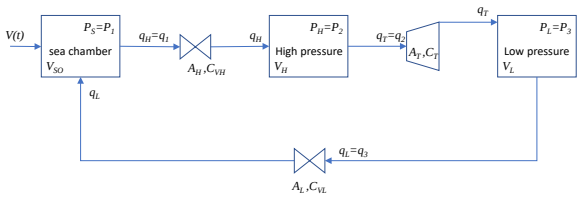

Figure 2. Schematic of lumped parameter model of CCPTO.

OWC structure installed into the breakwater at the entrance to the port of Mutriku, Spain. It is the world's first multi-turbine, wave energy facility and was first connected to the grid in 2011. The breakwater consists of 16 air chambers. In each chamber, an open cycle OWC system has been fitted with an 18.5kW Wells fixed-pitch turbine, giving a total capacity to the plant of 296kW. By targeting this specific facility, the sizing of the CCPTO system is limited by real-world dimensions. These constraints reduce the design space and provide more concrete conclusions about the sensitivity of the power output.

2. MODELLING

The pneumatic system of the CCPTO is shown schematically in Fig. 2. The governing equations are formulated in terms of mass flow rate so that the modelled variables in the differential equations are the mass in each chamber. A previous formulation in terms of chamber pressure should be equally valid as implemented by Vicente et al. (2017), but in the current study it was found to yield slowly divergent total pressure. It may be that the presence of damping in their system of equations is stabilising the model. In contrast in the current formulation the conservation of mass is implicitly satisfied at each instant, and hence the solutions are stable in the long term, even though the pneumatic system is treated in isolation.

2.1. Assumptions

The CCPTO is idealised as a closed pneumatic system, as shown in Fig. 2. The instantaneous mass in each chamber is determined from the sum of the mass flux through the valves and turbine. The mass flow rates are obtained from the volumetric flow rates, which depend on the instantaneous pressures in the system. This 1D model is crude as it excludes the full complexity of the internal flow and it is based on a number of assumptions:

- isentropic compression/expansion is assumed in all chambers;

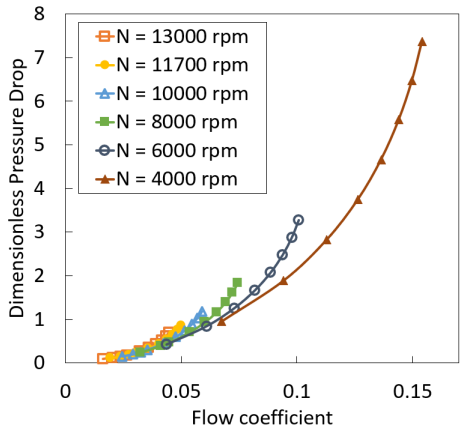

Figure 3. Variation of pressure drop with flow coefficient for different rotational speed of a proposed turbine suitable for the CCPTO

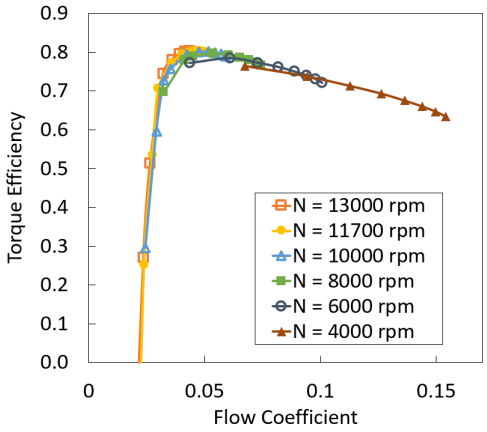

Figure 4. Variation of efficiency with flow coefficient for different rotational speed of a proposed turbine suitable for the CCPTO

- the sea surface acts as a rigid piston, so no sloshing is considered;
- air density at valves and turbines is assumed to be equal to the upstream value;
- a rudimentary turbine model is adopted. In effect the turbine is represented as an orifice, with and area A_T and a turbine coefficient, C_T.

In fact, detailed RANS assessment of a suitable axial flow turbine shows that this last assumption is quite good, for a given rotational speed. Nonetheless, care is needed when exploring the effect of the turbine size implicit in A_T, as this is effectively a tuned model. Although the full presentation of the preliminary design of the proposed air turbine exceeds the scope of this paper, the main results are shown Fig. s 3 and 4. The pressure drop and the torque efficiency are plotted depending on the flow coefficient for different rotational speeds. The variables are non-dimensionalized as follows (see Falcão et al. (2018)):

Dimensionless pressure drop:

$$\Psi = \frac{\Delta P}{\rho \Omega^3 D^5} \tag{1}$$

Flow coefficient:

$$\Phi = \frac{Q}{\Omega D^3} \tag{2}$$

Torque efficiency:

$$\nu = \frac{\tau \Omega}{\dot{m} C_p T_{01} (1 - \frac{p_{03}}{p_{01}}^{\frac{\gamma - 1}{\gamma}})} \tag{3}$$

where ΔP is the pressure drop across the turbine, ρ is the air density, Ω is the rotational speed in radians per unit time, Q is the volume flow rate, D is the rotor diameter, τ is the torque, $\dot{m}$ is the mass flow rate, C_p is the air heat capacity, γ is the heat capacity ratio, T_{01} is the inlet total temperature, P_{01} and P_{03} are respectively the inlet and outlet total pressures.

The non-dimensionalization of the pressure drop curves for different rotational speeds collapse (Fig. 3) yields an envelope curve which follows a quadratic tendency, supporting the choice of a simple orifice model for the turbine. Fig. 4 shows a peak of the turbine efficiency around 80 %. However, the efficiency remains high when the flow characteristics are slightly modified. A certain adaptability of the turbine seems to be possible through tuning of the rotational speed, although the extend of that possibility remains to be investigated.

2.2. Governing Equations

The mass in each chamber can be decomposed into a mean and fluctuating component:

$$M_i = m_{i0} + m_i \tag{4}$$

where $i = 1,2,3$ for sea, high pressure and low pressure chambers, respectively. Assuming the system starts at atmospheric conditions, the initial mass in each chamber is given by:

$$m_{i0} = \frac{V_{i0}}{\rho_0} \tag{5}$$

The principal solution variables are given by the first order ordinary differential equations which simply enforce mass conservation (equation 6, 7, 8).

Sea Chamber mass flux:

$$\frac{dm_1}{dt} = q_3 - q_1 \tag{6}$$

High Pressure Chamber mass flux:

$$\frac{dm_2}{dt} = q_1 - q_2 \tag{7}$$

Low Pressure Chamber mass flux:

$$\frac{dm_3}{dt} = q_2 - q_3 \tag{8}$$

The density in each chamber is simply the mass divided by the volume:

$$\rho_i = \frac{M_i}{V_i} \tag{9}$$

The volumes, V_i, of the high and low pressure chambers are fixed and the volume of the Sea Chamber is determined by the instantaneous water level:

$$V_1 = V_{10} + V_S(t) \tag{10}$$

$$V_{2,3} = V_{20,30} \tag{11}$$

The entire system is driven by the perturbation from equilibrium of the sea volume in the sea chamber caused by the oncoming waves. This will be discussed in section 2.3.

The flow rates in the system are obtained by treating both valves and the turbine as a simple flow restriction. It is given by:

$$q_i = C_i A_i \sqrt{2\rho_i} \Re\left(\sqrt{P_i - P_{i+1}}\right) \tag{12}$$

where C_i is a discharge coefficient and A_i is proportional to the open area of the component. Note that if the pressure difference is negative (i.e. $P_{i+1} > P_i$), the flow rate is 0. The density, ρ is assumed to be that of the upstream chamber, but this could be relaxed to be either an average of up- and downstream values or simply set to the reference value. Note that no account is taken of the shape of the ducting close to the valves or turbine. The effect of turbulence, flow separation and irrecoverable pressure drop are embedded in the assumed discharge and turbine coefficients.

The instantaneous pressure is required in each chamber to calculate the flow rates. This is calculated on the basis of an isentropic process. It is assumed that the entire system starts at a pressure equilibrium conditions (e.g. the pressure and volume and density are atmospheric):

$$P_i = P_0 \left(\frac{\rho_i}{\rho_0}\right)^{\gamma} \tag{13}$$

2.3. Modelling of incoming waves

The volume of air in the sea chamber $V_S(t)$ depends both on the incoming waves i.e. the OWC motion, and on the back pressure P_1 imposed by the CCPTO. The coupling is achieved by solving the following differential equation:

$$m_{wc}\frac{d^2z}{dt^2} + R\frac{dz}{dt} + Sz = F_S + F_w + F_g \tag{14}$$

where $z(t)$ is the water column elevation, so that $V_S(t) = -A_S \times z(t)$.

Equation 14 results from applying Newton's second law of motion to the water column of fixed mass m_{wc}, height H_{wc} and cross-sectional area A_S, subjected to the following list of forces.

Force exerted by the CCPTO back pressure:

$$F_S = P_1 A_S \tag{15}$$

Force exerted by the incoming waves:

$$F_w = -\rho_w g z_{sea} A_S \tag{16}$$

Damping accounting for the water/walls friction losses:

$$R = \frac{1}{2}\rho_w V_m^2 A_{wc} C_f \tag{17}$$

The damping term R represents losses due to friction between the water column and the concrete walls of the chamber. ρ_w is the water density, taken constant, V_m is the water column mean velocity, A_{wc} is the contact surface area and C_f is a friction coefficient approximated using a correlation with the Reynolds number of the flow. The prime role of this damping term is to have a better understanding of the dynamic response of the system using a reasonable value for losses.

Finally, the hydrostatic forces to account for weight of the water column and buoyancy forces are included. As these last two forces obviously don't change, together they represent the equilibrium sea level and so effectively define the sea chamber volume V_{10}. They are included to allow the easy application of different tide heights.

$$F_g = m_{wc} g \tag{18}$$

$$S = \rho_w g A_S \tag{19}$$

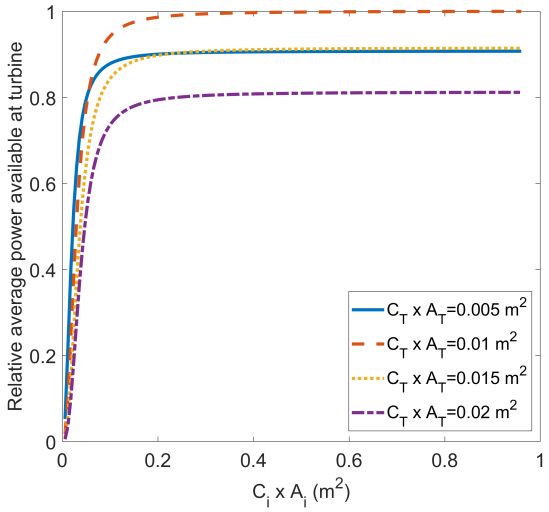

Figure 5. Variation in power with valve size metric $C_i \times A_i$ for different turbine size metrics $C_T \times A_T$.

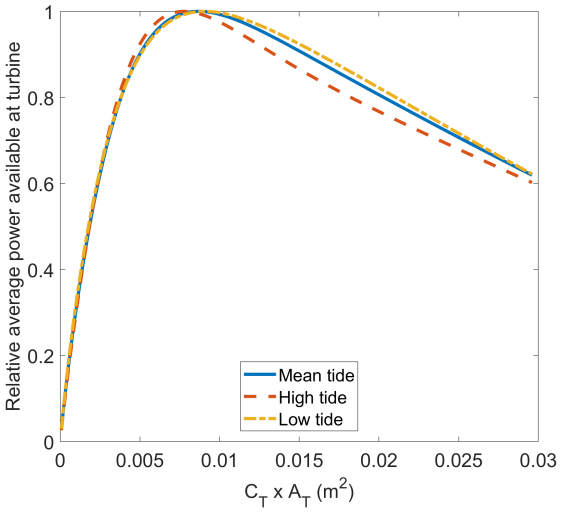

Figure 6. Variation in power with turbine size metric $C_T \times A_T$ for different tides.

When monochromatic waves are used in section 3, the sea level outside the sea chamber is assumed to vary regularly following a sinusoidal pattern as follows:

$$z_{sea}(t) = H_{wc} + Zsin(2\pi ft) \tag{20}$$

where Z and f are the incoming waves height and frequency respectively. They reflect the local wave climate. When polychromatic waves are used in section 4, a sample extracted from measurements in Mutriku is used for $z_{sea}(t)$.

3. INITIAL SIZING

As previously mentioned, this study focuses on a fixed OWC structure installed into a breakwater in the port of Mutriku, Spain. The sizing of the CCPTO is therefore constrained by the real-world dimensions of the Mutriku chambers. The gross size of the sea chamber is already fixed between 100 and 200 m^3 depending on the tide. The low and high pressure chambers are also limited by the turbine hall scale. Assuming they have the same size, they cannot exceed 90 m^3 each. There may be an advantage to having a larger HP chamber with the LP chamber vented to atmosphere, effectively making he LP volume infinite. This is beyond the scope of the current study and will be considered in future work.

The sensitivity of the power output to the size of valves and turbine is assessed using a sinusoidal monochromatic wave as presented in equation 20. The wave height and period are taken here as the most common in Mutriku's wave climate: $Z = 1.5\ s$ and $T = 1/f = 10\ s$. The areas A_i and A_T in equation 12 do not necessarily represent the geometric areas of the valves and turbine, as there is uncertainty on the value of the discharge coefficients C_i and C_T, but nonetheless it represents a metric of the relative size. The results are thus presented for $C_i \times A_i$ and $C_T \times A_T$ rather than A_i and A_T in Fig. 5 and 6.

3.1. Valves

Fig. 5 presents the average power available at the turbine depending on the valves size, for different turbine sizes, at mean tide. The power is non-dimensionalized by the maximal power, obtained here for $C_T \times A_T = 0.01\ m^2$. The two valves are assumed to be identical. Whatever the turbine size, the power increases with the valves size until it reaches a plateau. For $C_i = 0.6$, the threshold is here attained around $A_i = 0.4\ m^2$. Indeed, once the valves are big enough compare to the turbine, they do not limit the air flow and thus do not impact the power output. The actual value of this threshold is somewhat subjective; however in Mutriku the opening of the sea chamber is $0.5\ m^2$ and so the maximum size of the valves will be of this order. As a result, this might not be a limiting design issue.

3.2. Turbine

An optimum is expected to exist for the turbine size. Indeed, two competing phenomena occur simultaneously: on one hand, the mass flow increases with the turbine area, thus increasing the power output; on the other hand the pressure drop decreases when the turbine area increases, thus decreasing the power output. To investigate those opposing effects, the average power available at the turbine depending on

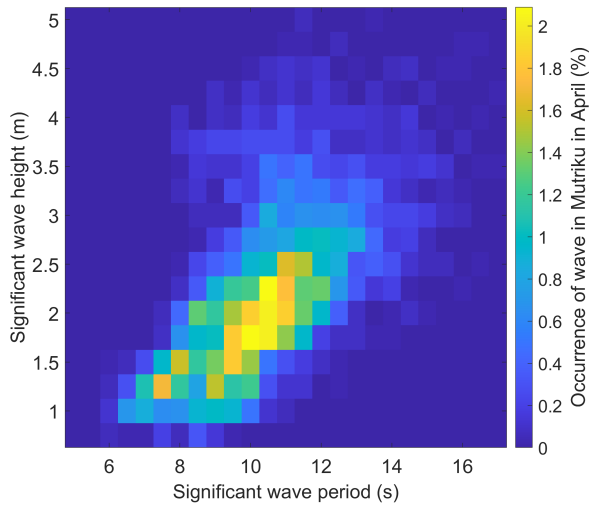

Figure 7. Mutriku wave climate in a month of April.

the turbine size is plotted Fig. 6 for low, mean and high tides. The power is non-dimensionalized by the maximal power for each tide. As the turbine size increases, the power output first increases sharply till it reaches a maximum, then it decreases more gently. The optimum is reached at around $A_T = 0.013\ m^2$, although it varies a little depending on the tide. Here again the actual value is uncertain as the discharge coefficient was arbitrarily taken as $C_T = 0.74$, based on the data in Fig. 3. Moreover, it is unclear how this area A_T relates to the aperture area of an actual turbine.

4. SENSITIVITY TO THE SEA STATE

4.1. Polychromatic wave climate

Measurements of the internal free surface heights in the sea chamber at Mutriku for 30 days of a month of April were made available by the operators through private communication. These measurements were taken as an open-cycle PTO system was in place. They are here assumed to be reasonably representative of the open sea behaviour. The significant wave period and height were calculated using the spectral moment method as described by Chun and Suh (2018). Fig. 7 presents the resulting wave climate showing the probability of any given sea state to occur in Mutriku in April. Note that the pair $[1.5\ m, 10\ s]$ which was used for the initial sizing in section 3 is the centre bin of the wave climate.

4.2. Effect of the tides

To investigate the effect of the sea state and the tides on the expected power output, the model was

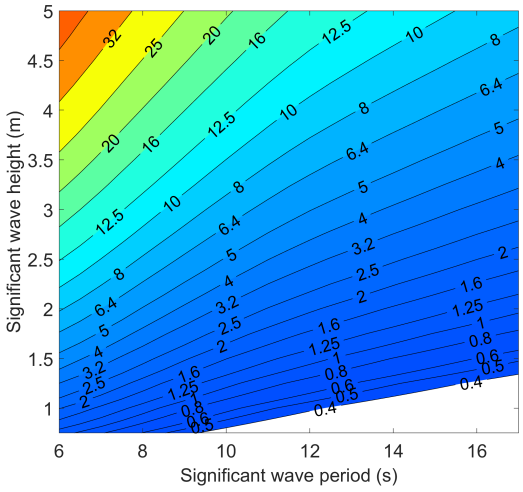

(a) Average power at turbine for high tide (kW)

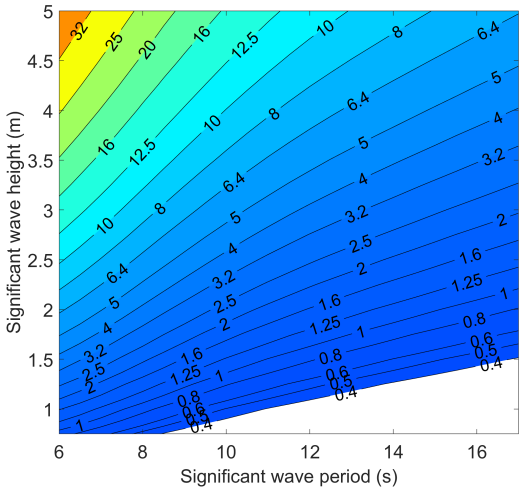

(b) Average power at turbine for mean tide (kW)

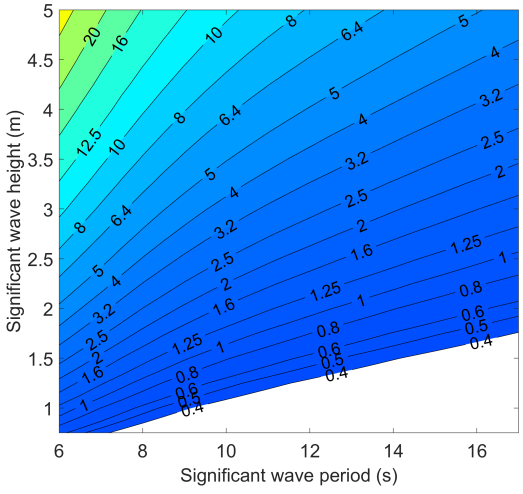

(c) Average power at turbine for low tide (kW)

Figure 8. Average power available at turbine for a polychromatic wave input of different standard height and period, for different tides.

run using a polychromatic wave input instead of the monochromatic sinusoidal wave used in section 3. To do so, a 1000 s sample was extracted from the measurements carried out in Mutriku's sea chamber. The high frequency components are filtered out to prevent unwanted noise. The sample is scaled to each of the wave height and period, and then used as the z_{sea} input to the model. The resulting average power and standard deviation of power matrices are respectively shown Fig. 8 and 9 for low, mean and high tides. For this work, the valve size was chosen big enough to be on the plateau of Fig. 5, and the turbine size was chosen close to the maximum efficiency of Fig. 6, (i.e. so that $C_T \times A_T = 0.01\ m^3$).

Although the actual values displayed in the power matrices in Fig. 8 are to be taken with caution considering the crudeness of the 1D model, it should be noted that the order of magnitude agrees with the measured electric power actually generated by a turbine in Mutriku as reported by Ibarra-Berastegi et al. (2018, 2021). The global trend for all tides shows the highest power outputs for waves with the smallest periods and the biggest heights. Indeed for these wave periods and heights, the air is pushed through the turbine more frequently and with a higher compression ratio. The three graphs are drawn with the same colour values so as to highlight the effect of the tide on the power. For all sea states, a higher tide results in a higher average power. This can be explained by a smaller sea chamber volume of air at higher tide which make the incoming wave comparatively bigger and thus more effective.

The standard deviation of power plotted Fig. 9 is an important indication of how much the available power fluctuates around the average since the turbine will not be able to adapt for each wave. A major advantage expected from the Closed-Cycle PTO is the smoothing of the power fluctuations. The standard deviation present the same variation as the power itself: it is higher for smaller wave periods, taller waves, and higher tide. It varies from half of the average power for the highest powers, to 1.4 times the power for the lowest ones.

4.3. Energy output

The matrix presented in Fig. 10 is the product of the wave climate matrix from Fig. 7 with the power matrix obtained for mean tide from Fig. 8(b), multiplied by 720 h i.e. the number of hours in a month. It indicates how much energy is expected to be produced by each sea state for a month of April in Mutriku according to the model, if the tide was constant at mean value. The sum of the matrix is 2067 kWh; it represents the total energy expected to be produced in that month. More than the values themselves, the distribu-

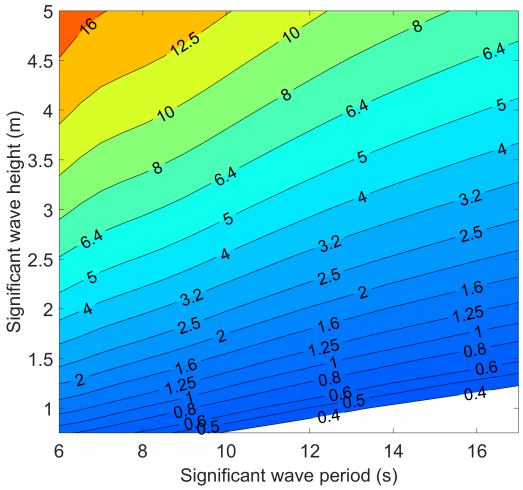

(a) Standard deviation of power for high tide (kW)

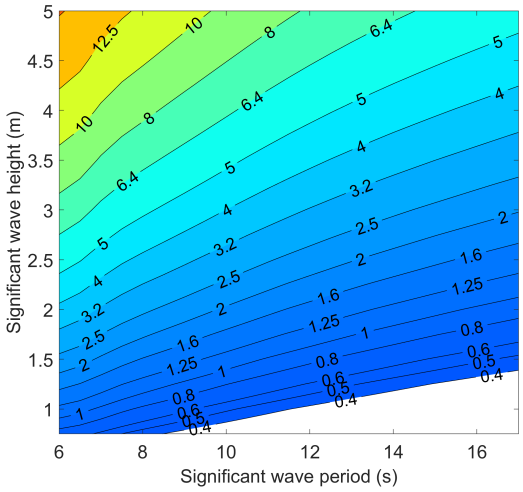

(b) Standard deviation of power for mean tide (kW)

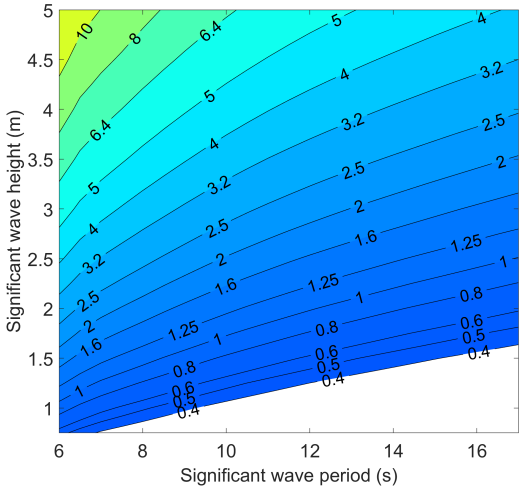

(c) Standard deviation of power for low tide (kW)

Figure 9. Standard deviation of power at turbine for a polychromatic wave input of different standard height and period, for different tides.

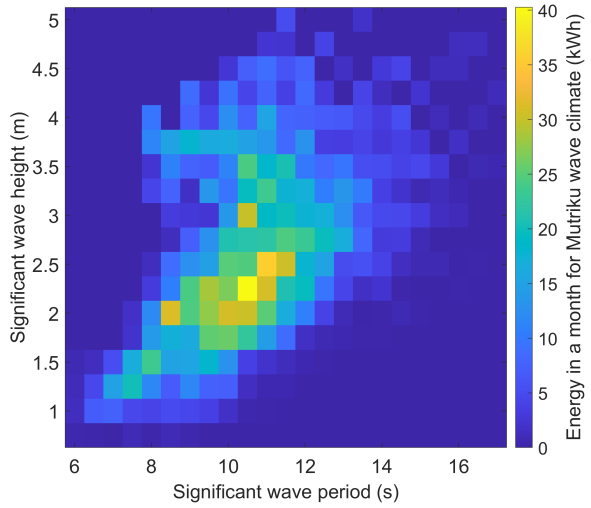

Figure 10. Energy produced in a month of April at mean tide for different waves in Mutriku.

tion of energy is an important result as it is in fact the design target of a suitable turbine for the CCPTO. For a constant low tide level, the average power would be 1.94kW; for mean tide it would be 2.87kW; and for high tide it would be 3.77kW. This suggests that while tide does affect the power production potential, the average power over the month will tend towards that obtained with constant mean tide.

5. CONCLUSION

In this article, a simple parameter model of the closed cycle power take off of an oscillating water column device has been presented and used to investigate the sensitivity of the power output of such a wave energy conversion system to geometric parameters and sea state variations. To settle the study in a concrete frame, the dimensions of the real-world Mutriku breakwater were used. By targeting this specific facility, the design space was constrained thus limiting the sizes of the sea chamber as well as the low and high pressure reservoirs. The sensitivity of the power output to the valve and turbine sizes was assessed using an ideal monochromatic wave input. It was found that a threshold exist for the valve size above which the power reaches a plateau; increasing the valves further is of no use. As for the turbine size, an optimal cross-sectional area exists. More realistic sea state conditions were then explored using polychromatic wave input extracted from measurements of the internal free surface height in Mutriku sea chamber. It was found that more power can be extracted for smaller wave periods, taller wave height and higher tide. Using the Mutriku wave climate calculated from measurements, a distribution of power expected to be produced for each Mutriku sea state was derived. This gives us a more accurate target for future turbine designs.

6. ACKNOWLEDGEMENT

The authors would like to acknowledge that part of their work was funded through the SEAI/RDD/495 Grant by the Sustainable Energy Authority of Ireland.

7. REFERENCES

P. Benreguig, V. Pakrashi, and J. Murphy. Assessment of primary energy conversion of a closed-circuit OWC wave energy converter. *Energies*, 12(10):1962, 2019.

H. Chun and K.D. Suh. Estimation of significant wave period from wave spectrum. *Ocean Engineering*, 163:609–616, 2018.

A.F.O. Falcão, J.C.C. Henriques, and L.M.C. Gato. Self-rectifying air turbines for wave energy conversion: A comparative analysis. *Renewable and Sustainable Energy Reviews*, 91:1231–1241, 2018.

F. Fusco, G. Nolan, and J.V. Ringwood. Variability reduction through optimal combination of wind/wave resources – an irish case study. *Energy*, 35(1):314–325, 2010.

J.C.C. Henriques, J.C.C. Portillo, L.M.C. Gato, R.P.F. Gomes, D.N. Ferreira, and A.F.O. Falcão. Design of oscillating-water-column wave energy converters with an application to self-powered sensor buoys. *Energy*, 112:852–867, 2016.

G. Ibarra-Berastegi, J. Sáenz, Al. Ulazia, P. Serras, G. Esnaola, and C. Garcia-Soto. Electricity production, capacity factor, and plant efficiency index at the mutriku wave farm (2014–2016). *Ocean Engineering*, 147:20–29, 2018.

G. Ibarra-Berastegi, A. Ulazia, J. Sáenz, P. Serras, S. J. González Rojí, Ganix Esnaola, and G. Iglesias. The power flow and the wave energy flux at an operational wave farm: Findings from mutriku, bay of biscay. *Ocean Engineering*, 227:108654, 2021.

M. Vicente, P. Benreguig, S. Crowley, and J. Murphy. Tupperwave - preliminary numerical modelling of a floating owc equipped with a unidirectioal turbine. In *Twelfth European Wave and Tidal Energy Conference*, 2017.